JACS
JOURNAL OF THE AMERICAN CHEMICAL SOCIETY
Article
pubs.acs.org/JACS

Crystallization of Methyl Ammonium Lead Halide Perovskites: Implications for Photovoltaic Applications

Yaron Tidhar,[†] Eran Edri,[‡] Haim Weissman,[†] Dorin Zohar,[†] Gary Hodes,*[,‡] David Cahen,*[,‡] Boris Rybtchinski,*[,†] and Saar Kirmayer*[,‡]

Departments of [†]Organic Chemistry and [‡]Materials and Interfaces, Weizmann Institute of Science, Rehovot 76100, Israel

Supporting Information

ABSTRACT: Hybrid organic/lead halide perovskites are promising materials for solar cell fabrication, resulting in efficiencies up to 18%. The most commonly studied perovskites are $CH_3NH_3PbI_3$ and $CH_3NH_3PbI_{3-x}Cl_x$ where x is small. Importantly, in the latter system, the presence of chloride ion source in the starting solutions used for the perovskite deposition results in a strong increase in the overall charge diffusion length. In this work we investigate the crystallization parameters relevant to fabrication of perovskite materials based on $CH_3NH_3PbI_3$ and $CH_3NH_3PbBr_3$. We find that the addition of $PbCl_2$ to the solutions used in the perovskite synthesis has a remarkable effect on the end product, because $PbCl_2$ nanocrystals are present during the fabrication process, acting as heterogeneous nucleation sites for the formation of perovskite crystals in solution. We base this conclusion on SEM studies, synthesis of perovskite single crystals, and on cryo-TEM imaging of the frozen mother liquid. Our studies also included the effect of different substrates and substrate temperatures on the perovskite nucleation efficiency. In view of our findings, we optimized the procedures for solar cells based on lead bromide perovskite, resulting in 5.4% efficiency and V_{oc} of 1.24 V, improving the performance in this class of devices. Insights gained from understanding the hybrid perovskite crystallization process can aid in rational design of the polycrystalline absorber films, leading to their enhanced performance.

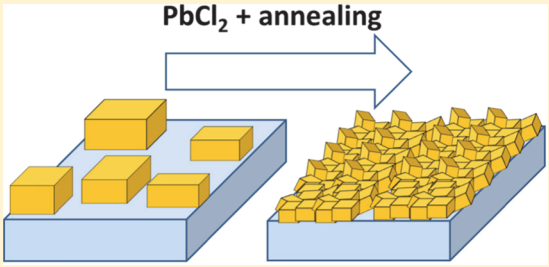

INTRODUCTION

Organic−inorganic solar cells based on lead halide perovskites are drawing growing interest recently due to their high efficiency, low fabrication cost (solution processing), and tunability of their optical properties.[1−4] Since the introduction in 2009,[5] devices using these materials have evolved rapidly to yield efficiencies of about 18%[6] (at the time of writing) for small contact area devices. The most commonly used perovskite was $CH_3NH_3PbI_3$ ($MAPbI_3$). It was found that the presence of $PbCl_2$ in the deposition solution improved the photovoltaic properties of the perovskite, mainly by increasing the electron diffusion length.[7,8] Remarkably, no significant chloride concentrations are found in the end product. In almost all studies, a mixture of $PbCl_2$ and excess CH_3NH_3I (MAI) in a 1:3 molar ratio in DMF solution was used, which yielded a very significant improvement in the quality of the perovskite polycrystalline films and orientation of the crystallites.[9]

The two materials systems, i.e., with and without $PbCl_2$ addition, have continued to show improved power conversion efficiencies through various film preparation techniques and solar cell designs (e.g., two-step liquid deposition on mp-TiO_2,[10] two-step vapor deposition of a thin film,[11] and thermal coevaporation[12,13]). Furthermore, the perovskite-based solar devices performed more efficiently if the mesoporous (mp) TiO_2 scaffold was replaced by mp alumina (on a compact TiO_2 layer).[14] This is despite the fact that injection of the photogenerated electrons into the alumina is not considered to be possible due to the very wide alumina bandgap and low alumina electron affinity, so that the electrons need to move through the perovskite to reach the electron conductor, TiO_2. From these reports it is clear that the film deposition, involving perovskite crystallization, has a critical influence over the film morphology and, consequently, on the cell performance.[15]

Crystallization is a complicated process and is of key importance in many fields.[16,17] It is widely recognized that crystallization takes place via a stepwise route, which starts from a relatively slow nucleation step, followed by a faster growth process.[18−20] The nucleation can occur in the crystallizing phase with no external interactions;[16] this is known as homogeneous nucleation. Heterogeneous nucleation occurs when the critical nucleus is formed on an impurity, an interface, or other inhomogeneity present in the system.[16,21] Heterogeneous nucleation strongly influences the formation kinetics of crystals and polycrystalline films[22] and is in general more efficient than homogeneous nucleation. Increasing the availability of heterogeneous nucleation sites interacting with a supersaturated solution can greatly increase the rate at which crystals nucleate.[22]

While crystallization is very important in general, it seems to be particularly so for the perovskite cells, where the deposition from solution results in heterogeneous polycrystalline films,

Received: June 7, 2014
Published: August 29, 2014

 © 2014 American Chemical Society

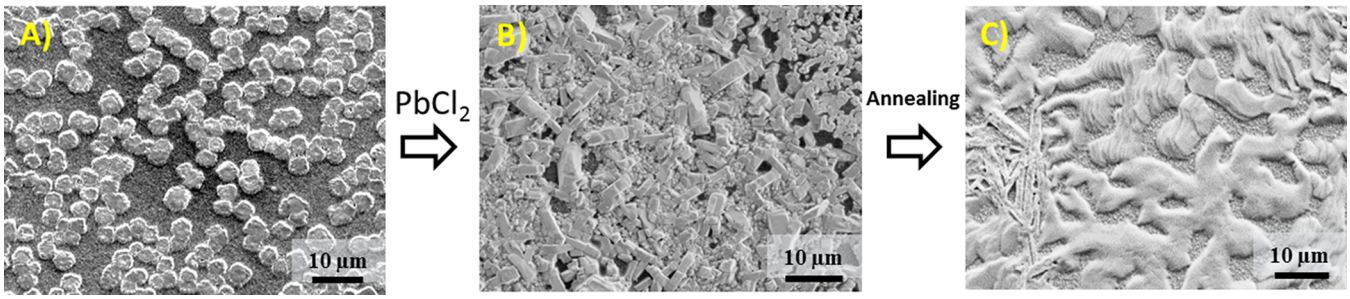

Figure 1. SEM images of perovskite films deposited on dense TiO_2 from DMF: (A) $MAPbI_3$ deposited at 70 °C substrate temperature (1:1 MAI:PbI_2), showing isolated crystals. (B) $MAPbI_{3-x}Cl_x$ (3:1 MAI:$PbCl_2$), deposited at 20 °C substrate temperature and placed under vacuum overnight, showing a dense layer of smaller nonoriented crystals. (C) $MAPbI_{3-x}Cl_x$ (3:1 MAI: $PbCl_2$) deposited at 70 °C substrate temperature and annealed at 120 °C for 45 min, showing large fused crystalline islands.

whose morphology determines the solar device performance. In this study, we aimed at elucidating the factors that define crystalline morphology of the solution-deposited perovskites, especially the role of Cl ions. The crystallization of two perovskite systems has been studied, namely methylammonium lead bromide ($MAPbBr_3$) and methylammonium lead iodide ($MAPbI_3$). We find that most of the morphological differences encountered during fabrication of perovskite polycrystalline films can be attributed to the perovskite nucleation process. Thus, controlling the extent as well as the location (i.e., in solution or on a surface) of the nucleation can help control the morphology and uniformity of the formed layers, resulting in improved photovoltaic device performances.

■ RESULTS AND DISCUSSION

The Role of $PbCl_2$ in the Nucleation and Growth Processes. As previously reported,[7,14,15,23] the addition of $PbCl_2$ to the precursor solution has a profound effect on the morphology, leading to improved performance of the perovskite photovoltaic devices. Adding $PbCl_2$ appears to increase the crystal domain size, induce a preferred orientation in the deposited film, and increase the electron diffusion length.[7,24] These effects can also be achieved by introducing chloride as MACl instead of $PbCl_2$ in the precursor solution.[9] The question remains, though, what is the role that the $PbCl_2$ plays in the synthesis. To answer this question, we compared the crystallization processes with and without added $PbCl_2$.

Equimolar Iodide Case. Spin-casting an equimolar solution of MAI and PbI_2 in DMF on a flat TiO_2 substrate (i.e., without any mesoporous scaffold), initially yields a transparent film with a yellowish tint. Heating the substrate to 60 °C for a few minutes transforms the film color to a dark brown (almost black). Scanning electron microscopy (SEM) imaging reveals the formation of micrometer-long needles ranging from hundreds of nanometers to several micrometers in diameter (Figure S1 in the Supporting Information). The density and coverage in this system is a function of the substrate roughness and temperature, as will be discussed below. A 3:1 MAI and PbI_2 case was studied as well (see below).

Mixed Iodide-Chloride Case. A mixed halide solution is prepared by mixing a 3:1 molar ratio of MAI to $PbCl_2$ in DMF, using conditions typically employed in solar cell fabrication.[15] For concentrations used in device fabrication (30−40% by weight), a MAI:$PbCl_2$ ratio lower than 3:1 results in incomplete dissolution of the lead salt. Upon deposition of the 3:1 solution on a substrate, a transparent yellowish film is formed. When placed on a hot plate (100−120 °C; annealing, customarily employed in perovskite cell fabrication), the film changes color to red (occasionally), then to a deep yellow, followed by deep black (over a period of minutes). The annealing process will be discussed below. SEM images of such layers show that the morphology is dramatically different from that obtained when $PbCl_2$ is not involved in the fabrication (Figure 1). While using $PbCl_2$, large, interconnected domains are formed (Figure 1C), needle-like (room temperature substrate, Figure S1) or mainly isolated separate crystals (70 °C substrate, Figure 1A) are formed in the $PbCl_2$-free synthesis. In addition, although the precursor solution contained more than 20 mol % chloride, only traces could be detected in the fabricated film. Energy dispersive spectroscopy in the SEM and X-ray photoelectron spectroscopy (XPS) showed that the amount of chloride in the film is minute and usually below the sensitivity threshold of the measuring technique/instrument. Thus, it appears that in the case of $MAPbI_3$, the $PbCl_2$ addition affects the crystal formation kinetics as it is not a part of the final phase, except, possibly, at trace concentrations. While the diffractograms of the $MAPbI_3$ and $MAPbI_{3-x}Cl_x$ films are similar (Figure S2), their comparison clearly shows that the "mixed halide" films exhibit preferred orientation at the (110) direction with the *c*-axis normal to the substrate, as has been reported before.[12,14] Since the annealing process dramatically changes the crystal morphology, we need to separate the effects of the thermal treatment from those of the solution deposition. Figure 1C shows an SEM image of a spin-coated film using 3:1 MAI:$PbCl_2$ DMF solution annealed at 120 °C for 45 min; Figure 1B shows a spin-coated 3:1 MAI:$PbCl_2$ film deposited from DMF that was dried under vacuum overnight at room temperature. The vacuum-dried sample was transparent at deposition and changed color to black within a few minutes, which agrees with its transformation to the perovskite structure. Removing the solvent from the film resulted in the formation of many small crystals scattered in a disordered polycrystalline layer. Examining the annealed film (Figure 1C) indicates that the small crystals formed upon deposition coalesce during the annealing process to yield large interconnected crystalline domains. Annealing of the lead iodide perovskite films in the absence of $PbCl_2$ lead to rather isolated crystalline domains (Figures S1 and S5C)

Equimolar Bromide Case. While $MAPbI_3$ perovskite can contain only very small amounts of chloride in the crystal structure,[25] the bromide analog has been reported to form a solid solution across a wide range of chloride concentrations.[26] Methylammonium lead bromide ($MAPbBr_3$) and bromide-

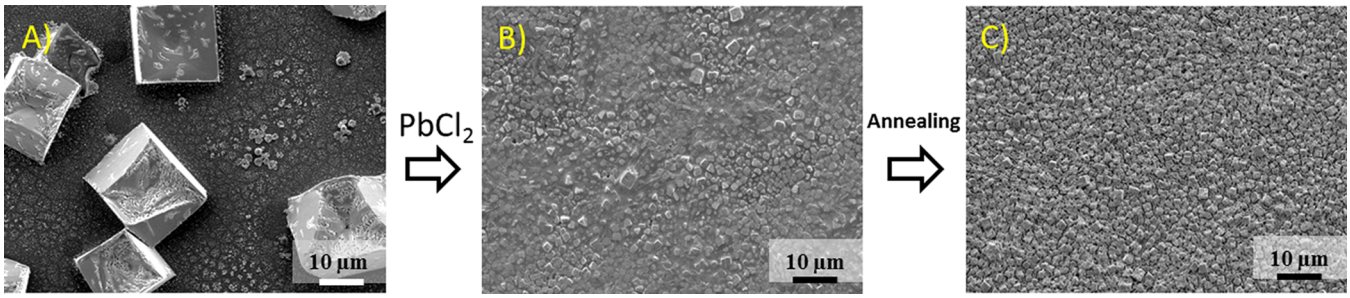

Figure 2. SEM images of perovskite films deposited on dense TiO_2 from DMF at 80 °C substrate temperature: (A) $MAPbBr_3$ showing very large isolated crystals, exhibiting surface coverage of <20%. (B) $MAPbBr_{3-x}Cl_x$ showing smaller crystals covered in part by excess organic material that did not evaporate under low pressure. (C) $MAPbBr_{3-x}Cl_x$ annealed at 160 °C for 45 min, showing smaller, close-spaced crystals exhibiting surface coverage of close to 100%.

chloride ($MAPbBr_{3-x}Cl_x$) are materials of particular interest for high open circuit voltage solar cells.[27,28] Spin-casting an equimolar solution of MABr and $PbBr_2$ in DMF on a flat TiO_2 substrate at room temperature, and heating to 80 °C to remove the solvent, results in the formation of an orange-colored layer. SEM images show large, tens of micrometer-sized cuboids with truncated facets (Figure 2A). These are scattered over the surface, exhibiting a very low surface coverage (between 10 and 50%, depending on substrate type and temperature, see below).

Mixed Chloride-Bromide Case. In contrast to the "Equimolar Bromide Case" (Figure 2A) if $PbCl_2$ is used, mixed with MABr in a 1:3 molar ratio in DMF and deposited on a substrate, at first a transparent pale yellow layer is formed (Figure 2B). After annealing at 150−160 °C, the transparent layer becomes deep lemon-yellow and then (in 30−60 min) vivid orange (Figure 2C). While XRD confirms that the material is $MAPbBr_3$ (see Supporting Information), the morphology and the surface coverage of this layer are very different from that obtained in the pure bromide case (Figure 2A). SEM images show that instead of micron-sized cubes, hundreds of nanometer-sized cubes are formed in a densely packed manner, resulting in a better surface coverage (Figure 2C). The transmission spectra of the two films on a flat substrate corroborate higher optical density of films formed from $PbCl_2$ and MABr (Figure S3). Therefore, although the two materials, $MAPbI_3$ and $MAPbBr_3$, have different crystal growth properties and different intermixing properties with Cl, $PbCl_2$ appears to play a similar role of increasing the surface coverage.

To verify that the observed effects are due to the presence of $PbCl_2$ and are not the result of the excess methylammonium salts in the precursor solution, the deposition processes were repeated using 3:1 MAI:PbI_2 and 3:1 MABr:$PbBr_2$. SEM images of the resulting films (Figure S5) reveal that the increase in organic salt content results in morphological changes (in comparison to equimolar) systems less significant than in the presence of $PbCl_2$.

Overall, the $PbCl_2$ addition leads to a much more pronounced decrease in crystal size, the increase in number of crystals, and, ultimately, in better surface coverage. We anticipated that this may be due to heterogeneous nucleation induced by the less soluble $PbCl_2$, remaining as particles in solution. To test this hypothesis, we studied the effect of $PbCl_2$ addition on the growth of perovskite single crystals in systems that allow the effect to be observed visually (the procedures are described in detail in the Supporting Information). In short, $MAPbBr_3$ crystals were grown from equimolar solutions in DMF (similar to the ones deposited on substrates for the solar cell production) by slow vapor mixing of alcohols into the DMF solution. The $MAPbI_3$ crystals were grown by a modified version of a published procedure.[29] In the modified procedure, the concentrated solution was cooled to room temperature and was placed in a close vial under isopropanol vapor. Here, the slow exchange of the solvent (accompanied by decrease in polarity) induced the crystallization rather than a temperature change, as in the original method (see Supporting Information for details). The $PbCl_2$ content in these solutions was gradually increased from 1 to 10 mol % by mixing an equimolar solution with a second mixed halide solution (the two solutions were mixed to give the desired $PbCl_2$ concentration, prior to the vapor mixing process). These experiments showed that increasing amounts of $PbCl_2$ in the precursor solution for both types of crystals induces the growth of a larger number of crystals (Figures 3 and S4), and the first visual appearance of these crystals occurs faster under what are, except for the $PbCl_2$ concentration, otherwise identical conditions.

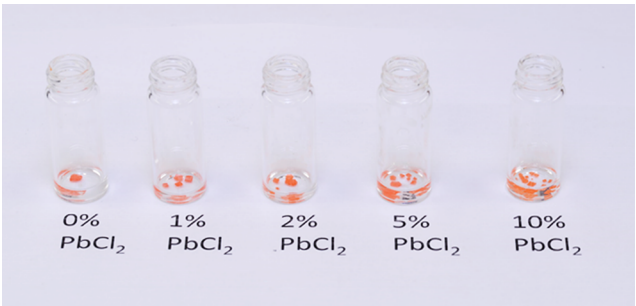

Figure 3. Crystallization product of $MAPbBr_3$ in vials containing increasing amounts of the mixed halide precursor solution. The number of the crystals increases with $PbCl_2$ concentration and the size of the crystals decreases.

Table 1. Summary of the Results of Crystallization Experiments, In Which Different Amounts of $PbCl_2$ Were Added to a Concentrated Perovskite Precursor Solution

percent of $PbCl_2$ out of all Pb precursor in the solution.	0%	1%	2%	5%	10%
number of single crystals formed: $MAPbBr_3$	1	6	10	10	16
number of single crystals formed: $MAPbI_3$	1	1	3	4	5

These observations are consistent with the idea that $PbCl_2$ provides heterogeneous nucleation sites for the crystallization of perovskite crystals. The solubility of lead halides in organic solvents increases with increase in the ionic radius of the halide, due to the decrease in Pb-halide bond strength (based on lead-halide, Pb-X, bond strength; Table 2) and better solvation of larger ions with diffuse charge density. Therefore, $PbCl_2$ is the least soluble Pb-halide in the DMF solutions. We note that there could be also a kinetic effect, i.e., slower dissolution of $PbCl_2$ in DMF that can lead to the presence of $PbCl_2$ particles. However, in all experiments described here, a visibly clear solution was used for spin-coating. Furthermore, using a 2-week aged solution yielded similar film morphology as a fresh solution. Also, filtering the solution (through a 0.22 μm filter) did not affect the morphology. We envisaged that due to its lower (or slower) solubility, small $PbCl_2$ nanoparticles are present in the DMF precursor solutions, inducing the nucleation of perovskite crystals. Larger number of nucleation sites eventually leads to smaller crystals and better coverage upon spin-coating.

Table 2. Lead-Halide Bond Strengths (values from ref 30) and Solubilities (at room temperature)

bond	D (kJ/mol)	solubility in DMF (g/mL)
Pb−Cl	243	0.08 ± 0.01
Pb−Br	201	0.17 ± 0.02
Pb−I	142	0.36 ± 0.01

Direct evidence for the involvement of $PbCl_2$ nanoparticles in the crystallization process comes from cryo-TEM studies of the precursor solution in DMF. In a typical experiment, 5 μL 3:1 MAI:$PbCl_2$ DMF solution or 1:1 MAI:PbI_2 DMF solution were spread over TEM grids and vitrified by plunging the grid into liquid nitrogen. Importantly, in cryo-TEM sample preparations, vitrification, taking place upon instantaneous cooling, is known to capture the solution-phase state, preventing processes occurring upon slower cooling or drying.[31,32] At first, no indication of nanoparticles was observed, possibly due to low contrast difference between the solution and the particles. However, in the 3:1 MAI: $PbCl_2$ case, when the sample was allowed to warm up to 153 K (from 77 K) under high vacuum, the solvent sublimed and nanoparticles ranging from 3 to 20 nm in diameter were observed to be uniformly spread within amorphous material over the entire imaged areas (Figure 4A,B). No such particles were detected in the 1:1 MAI:PbI_2 case. Electron diffraction patterns (Figure 4C and Table 3) indicated that these are $PbCl_2$ nanoparticles, supporting the occurrence of heterogeneous nucleation induced by $PbCl_2$. These observations were also corroborated using dynamic light scattering (DLS), revealing presence of ca. 10 nm particles in the filtered precursor solutions containing $PbCl_2$. We note that it is possible that the initial $PbCl_2$ nuclei grow to some extent (nucleating their own growth). However, these crystals would continue to react with the MAI, also leading to enhanced growth of $MAPbI_{3-x}Cl_x$ phase due to heterogeneous nucleation.

Table 3. Comparison of the Measured d-Spacings (in Å) to the ICSD (X-ray) Diffraction Data for $PbCl_2$ and PbI_2

PbI_2	$PbCl_2$	e-diffraction
6.89	6.16	6.21
3.94	3.75	3.42
3.49	2.92	3.04
2.27	2.64	
2.20	2.20	2.25
2.00	2.10	2.12

The Effect of Substrate Temperature and Texture. Surface roughness and temperature of the substrate are also important in determining the efficiency and rate of the nucleation and growth processes. The effect of the substrate temperature as well as of the annealing temperature on the morphology of the crystalline films were reported before, although these effects were not correlated with the crystallization pathway.[15,33,34] While examining the formation of $MAPbBr_3$ on mesoporous Al_2O_3, we noted that the substrate temperature is directly correlated to the surface coverage of the polycrystalline film (better coverage at higher temperatures). To study the thermal effect, the surface temperature of the substrate was monitored using a noncontact thermometer (see Supporting Information) immediately before spin-coating. Figure 5 shows SEM images of $MAPbBr_3$ after deposition on

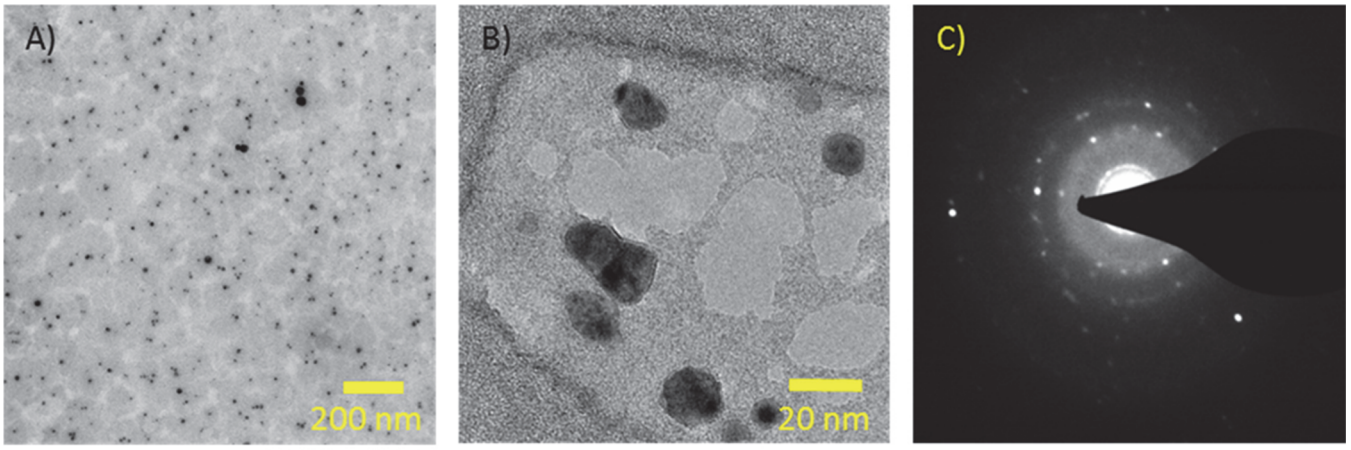

Figure 4. (A) TEM image of freeze-dried perovskite $MAPbI_{3-x}Cl_x$ precursor solution, showing an amorphous film (probably a mixture of the starting materials) with embedded $PbCl_2$ nanocrystals. (B) Higher magnification TEM image of the same freeze-dried perovskite precursor solution used for the e-diffraction shown in (C).

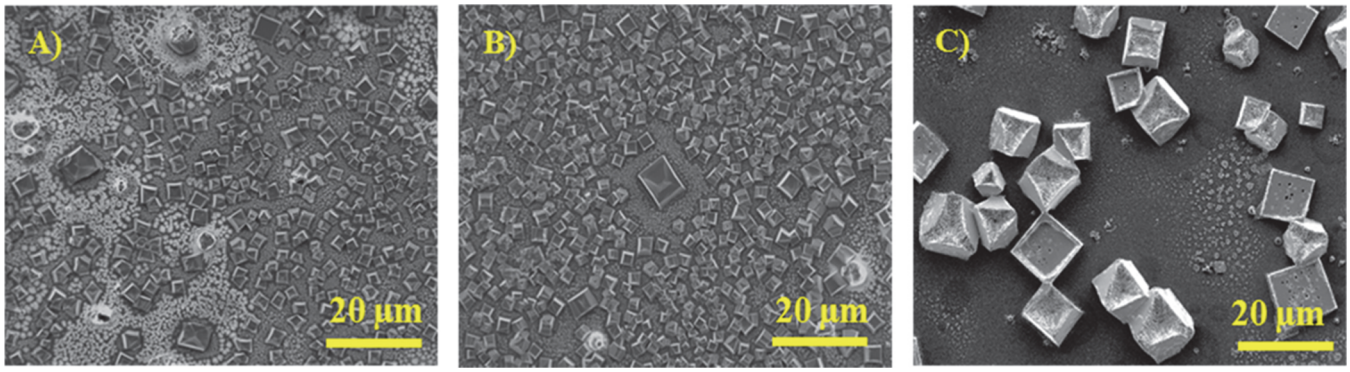

Figure 5. SEM images of $MAPbBr_3$ films formed on the surface of (A) mesoporous Al_2O_3 at room temperature; covered area 25% and (B) mesoporous Al_2O_3 heated to 60 °C; covered area 41%, (C) on the surface of dense TiO_2 heated to 60 °C; covered area 10%. All samples were annealed at 100 °C for 30 min after coating.

substrates at different temperatures ranging from 25 to 60 °C, followed by annealing at 100 °C for 30 min. The latter is commonly applied during solar cell fabrication in order to remove volatiles; it does not significantly influence the morphology of $MAPbBr_3$. The size of the crystals decreases and the number density increases as the substrate temperature increases. Thus, the substrate surface temperature during the casting of the film affects the degree of surface-induced nucleation: as the temperature is increased, so does the number of nucleation events,[16,22] resulting in a larger number of smaller crystals and better surface coverage. It is typical that the nucleation process has a higher activation energy and therefore slower rate than the following growth process. Temperature increase leads to faster nucleation and, hence, higher number of crystals, resulting in denser, more uniform films.

A similar experiment was carried out with $MAPbI_3$ films, where the surface temperature at the casting stage was varied between 20 and 60 °C. However, in this case, the nucleation and growth had to be separated (see below). Since the surface-induced nucleation is temperature sensitive, it is restricted to the initial deposition time (from the moment of solution casting until the substrate cools down). Fast growth is achieved by placing the samples under vacuum for the removal of the solvent, without further annealing (to avoid coarsening and additional nucleation). This allows us to decouple the surface nucleation from any other form of nucleation and from the crystal fusion (coalescence) that takes place during the annealing. SEM images of the resulting films are presented in Figure 6. As before, the number of the crystallites increased dramatically with increase in surface temperature. However, in addition to the increase in crystallite density, the increase in the substrate temperature also affects the directionality of the crystal growth. Casting the precursor solution on a substrate that is at room temperature and removing the solvent by low pressure result in the crystals growing with the *c*-axis parallel to the surface. When a similar experiment is done on a hot surface, more nucleation sites are formed on the surface, which results in a large number of crystallites with different orientation. This effect can be attributed to the lower symmetry (tetragonal *I4/mcm*) of the $MAPbI_3$ crystals[29,35] that may allow for a preferred growth facet, as opposed to the high symmetry cubic $MAPbBr_3$ that will grow homogeneously regardless of the nucleation origin. Furthermore, $MAPbI_3$ has a reversible tetragonal-to-cubic phase transition at 54 °C[35] that can affect the growth pattern of the crystal. This may influence the overall morphology, however the cubic crystals return to the tetragonal phase upon cooling.[29,35]

When analyzing the combined effects of the process parameters on the dynamics of crystal growth, one should also take into account the type of surface on which the material is deposited. The roughness and inhomogeneity of the substrate may allow for lower energy pathways for nucleation, thus increasing the probability to overcome the energy barrier for nucleation and resulting in a better surface coverage. Thus, it is not surprising that changing the substrate from the dense, relatively flat TiO_2, to a mesoporous one (either mp-TiO_2 or mp-Al_2O_3) results in a dramatic increase in the number of crystallites formed on the surface (Figure 5A,B vs C) and better surface coverage. We note that apart from the surface area and morphology, surface−solution interactions and surface wetting can also influence the nucleation process. Addressing these interactions is a subject of ongoing research.

To further address the influence of the annealing on the film morphology and composition (loss of Cl), EDS analysis of $MAPbI_{3-x}Cl_x$ films annealed at 120 °C for 30, 45, and 60 min was performed (Table S1). It shows that the Cl content in the film is reduced with annealing time, which is also supported by time-dependent XRD data of the annealing process (Figure S9). Furthermore, EDS analysis of the evaporated organic salt, captured in an in situ study of the annealing process by air-SEM (Figure S8), identifies it as MACl. Thus, the annealing process appears to remove the excess organic precursor in the form of MACl (leading to loss of Cl) and brings about crystal coalescence, forming large crystalline domains. We believe that these two processes may lead to the improved charge carrier diffusion in the annealed material, as observed for devices based on $MAPbI_{3-x}Cl_x$.[7]

To demonstrate how understanding of the parameters regulating the film formation is implemented in a solar cell fabrication, high-voltage devices were fabricated from $MAPbBr_{3-x}Cl_x$ using the optimal (i.e., best coverage) crystallization conditions as described above. The full details of the device fabrication are given in the Supporting Information. In short, a 40.5 wt % solution of $MAPbBr_{3-x}Cl_x$ was prepared by mixing a 1:3 molar ratio of $PbCl_2$ and MABr in DMF. Planar TiO_2 substrates were dried on a hot plate set to 110 °C for 10 min. The temperature of the surface was monitored by a noncontact thermometer to be 80 °C at the time of perovskite solution-casting that involves spin-coating. The deposited layers were then annealed in air at 150 °C for 50 min. The devices were completed by depositing an organic hole

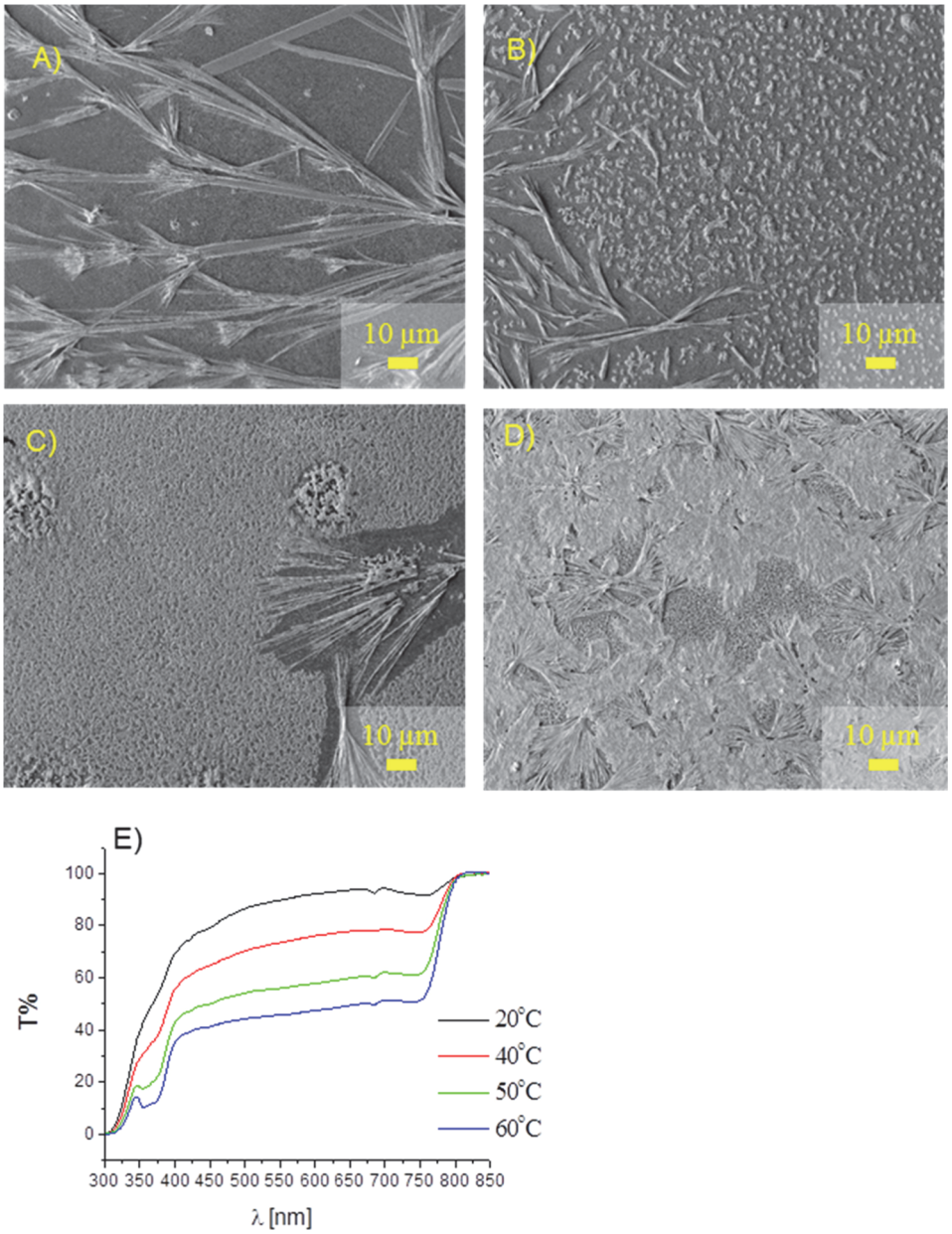

Figure 6. SEM images of $MAPbI_3$ films, spin-coated on the surface of dense TiO_2 at different substrate temperatures (solvent removed by low pressure, no annealing): substrate at (A) 20 °C; (B) 40 °C; (C) 50 °C; and (D) 60 °C. (E) Optical transmission measurements of $MAPbI_3$ perovskite films on dense TiO_2 layer, prepared by spin-coating on a substrate at different temperatures. The transmission spectra are reflection corrected and normalized to 100%.

conductor (CBP/LiTFSI),[24,27] and subsequent keeping in dry air for 12 h, followed by evaporating 80 nm thick gold layer as a back contact. The solar cell device characteristics are given in Figure 7. Controlling the layer morphology and improving its quality enabled a device exhibiting an open circuit voltage of 1.24 V, short circuit current of 7.8 mA cm^{-2}, FF of 56%, and 5.4% efficiency. This device exhibited nearly double the current density and substantially higher fill factor then previously reported $MAPbBr_{3-x}Cl_x$ high-voltage cells,[28] although at the cost of a reduced open circuit voltage. Importantly, a mesoporous (mp) scaffold was not required since high quality of the perovskite film was ensured by the proper crystallization conditions. Very recently a $MAPbBr_3$ solar cell with VOC up to 1.40 V and 6.7% efficiency has been reported (based on a mp-TiO_2 scaffold).[36]

■ CONCLUSIONS

Understanding crystallization processes pertinent to the formation of polycrystalline perovskite films allowed for a rationalization of the perovskite film preparation. By examining the effect of the different deposition processes in the context of crystal nucleation, we determined the role of each step in the preparation. It is apparent that mesoporous scaffolds offer more nucleation sites on the surface and hence contribute to a more uniform layer than flat substrates. Elevated temperature is needed to overcome the energy barrier for nucleation on any given substrate. We conclude from synthesis of single crystals of $MAPbI_3$ and $MAPbBr_3$ that $PbCl_2$ plays a key structural role in the crystallization process of these materials. We have established that due the low solubility of $PbCl_2$ in DMF, some fraction of it remains as inhomogeneities (nanoparticles)

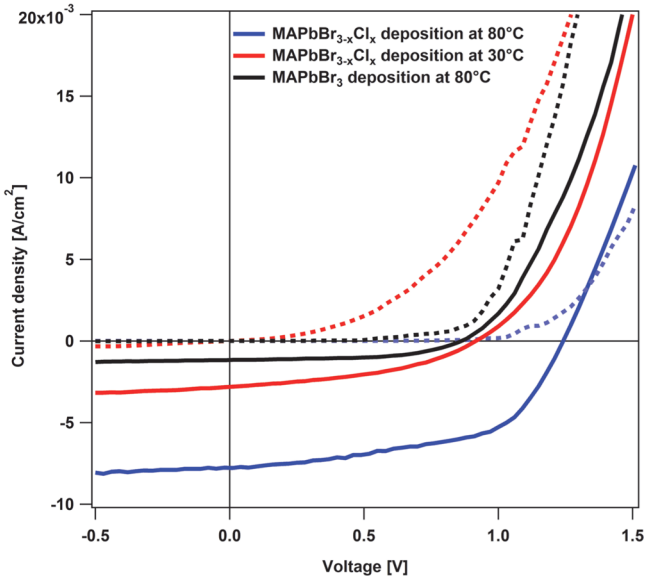

Figure 7. $J-V$ characteristics for planar $MAPbBr_{3-x}Cl_x$-based cells under standard AM1.5G illumination (100 mW cm^{-2}) (solid curves) and in the dark (dotted curves) for cell area of 0.04 cm^2. The measurements were made from −0.5 to 1.5 V in steps of 0.0 2 V with a waiting time of 200 ms between points. Black line: $MAPbBr_{3-x}Cl_x$ deposited on dense a TiO_2 substrate heated to 80 °C, followed by annealing at 150 °C for 45 min. Red line: $MAPbBr_{3-x}Cl_x$ deposited on a dense TiO_2 substrate heated to 30 °C, followed by annealing at 150 °C for 45 min. Blue line: $MAPbBr_3$ deposited on a dense TiO_2 substrate heated to 80 °C, followed by annealing at 150 °C for 45 min.

in the solution as shown by cryo-TEM. These nanoparticles act as heterogeneous nucleation sites for the perovskite crystals. This insight can explain the structural phenomena observed under the different conditions used to cast the films from solution during the fabrication of perovskite-based photovoltaic devices. Furthermore, we demonstrated that in $MAPbI_{3-x}Cl_x$ the annealing process removes the excess organic precursor in the form of MACl and drives the well-dispersed crystals to coalesce and form large oriented crystalline domains. These two processes lead, in our view, to the improved charge carrier diffusion. We also demonstrated the added value of a rational fabrication process by producing $MAPbBr_{3-x}Cl_x$ cells, which yielded 5.4% efficiency, roughly double our previously published efficiency for this material, although at a somewhat reduced V_{OC}.

■ ASSOCIATED CONTENT

Ⓢ Supporting Information

Additional experimental procedures, electron microscopic images, spectroscopic data, device fabrication procedures, and structural analysis data. This material is available free of charge via the Internet at http://pubs.acs.org.

■ AUTHOR INFORMATION

Corresponding Authors

saar.kirmayer@weizmann.ac.il
boris.rybtchinski@weizmann.ac.il
david.cahen@weizmann.ac.il
gary.hodes@weizmann.ac.il

Notes

The authors declare no competing financial interest.

■ ACKNOWLEDGMENTS

We thank the Leona M. and Harry B. Helmsley Charitable Trust, the Israel Ministry of Science's "Tashtiot", and the Weizmann-U.K. Joint Research Program (D.C., G.H.) for partial support. D.C. holds the Sylvia and Rowland Schaefer Chair in Energy Research. We also wish to thank the team at B-nano: Yaniv Brami, Yonat Milstein, and Rafi de Picciotto for their help with the in situ study of the $MAPbX_3$ annealing. We thank Tatyana Bendikov and Hagai Cohen for XPS analyses, and Ronit Popovitz-Biro for electron diffraction studies.

■ REFERENCES

(1) Nazeeruddin, M. K.; Gao, P.; Grätzel, M. *Energy Environ. Sci.* **2014**, *7*, 2448−2463.
(2) Park, N.-G. *J. Phys. Chem. Lett.* **2013**, *4*, 2423−2429.
(3) Hodes, G. *Science* **2013**, *342*, 317−318.
(4) Snaith, H. J. *J. Phys. Chem. Lett.* **2013**, *4*, 3623−3630.
(5) Kojima, A.; Teshima, K.; Shirai, Y.; Miyasaka, T. *J. Am. Chem. Soc.* **2009**, *131*, 6050−6051.
(6) National Center for Photovoltaics. *Best Research-cell Efficiencies Chart*; National Renewable Energy Labratory: Boulder, Colorado, USA, 2014; http://www.nrel.gov/ncpv/images/efficiency_chart.jpg.
(7) Stranks, S. D.; Eperon, G. E.; Grancini, G.; Menelaou, C.; Alcocer, M. J. P.; Leijtens, T.; Herz, L. M.; Petrozza, A.; Snaith, H. J. *Science* **2013**, *342*, 341−344.
(8) Edri, E.; Kirmayer, S.; Henning, A.; Mukhopadhyay, S.; Gartsman, K.; Rosenwaks, Y.; Hodes, G.; Cahen, D. *Nano Lett.* **2014**, *14*, 1000−1004.
(9) Zhao, Y.; Zhu, K. *J. Phys. Chem. C* **2014**, *118*, 9412−9418.
(10) Burschka, J.; Pellet, N.; Moon, S.-J.; Humphry-Baker, R.; Gao, P.; Nazeeruddin, M. K.; Grätzel, M. *Nature* **2013**, *499*, 316−319.
(11) Chen, Q.; Zhou, H.; Hong, Z.; Luo, S.; Duan, H.-S.; Wang, H.-H.; Liu, Y.; Li, G.; Yang, Y. *J. Am. Chem. Soc.* **2014**, *136*, 622−625.
(12) Liu, M.; Johnston, M. B.; Snaith, H. J. *Nature* **2013**, *501*, 395−398.
(13) Docampo, P.; Ball, J. M.; Darwich, M.; Eperon, G. E.; Snaith, H. J. *Nat. Commun.* **2013**, *4*, 1−6.
(14) Lee, M. M.; Teuscher, J.; Miyasaka, T.; Murakami, T. N.; Snaith, H. J. *Science* **2012**, *338*, 643−647.
(15) Eperon, G. E.; Burlakov, V. M.; Docampo, P.; Goriely, A.; Snaith, H. J. *Adv. Funct. Mater.* **2014**, *24*, 151−157.
(16) Dirksen, J. A.; Ring, T. A. *Chem. Eng. Sci.* **1991**, *46*, 2389−2427.
(17) Desiraju, G. R. *J. Chem. Sci.* **2010**, *122*, 667−675.
(18) Oxtoby, D. W. *Acc. Chem. Res.* **1998**, *31*, 91−97.
(19) Weissbuch, I.; Lahav, M.; Leiserowitz, L. *Cryst. Growth Des.* **2003**, *3*, 125−150.
(20) Chung, S.-Y.; Kim, Y.-M.; Kim, J.-G.; Kim, Y.-J. *Nat. Phys.* **2009**, *5*, 68−73.
(21) *The Theory of Transformations in Metals and Alloys*; Christian, J. W., Ed.; Pergamon: Oxford, 2002.
(22) Cacciuto, A.; Auer, S.; Frenkel, D. *Nature* **2004**, *428*, 404−406.
(23) Wojciechowski, K.; Saliba, M.; Leijtens, T.; Abate, A.; Snaith, H. J. *Energy Environ. Sci.* **2014**, *7*, 1142−1147.
(24) Edri, E.; Kirmayer, S.; Mukhopadhyay, S.; Gartsman, K.; Hodes, G.; Cahen, D. *Nat. Commun.* **2014**, *5*, 3461.
(25) Mosconi, E.; Amat, A.; Nazeeruddin, M. K.; Grätzel, M.; De Angelis, F. *J. Phys. Chem. C* **2013**, *117*, 13902−13913.
(26) Kitazawa, N.; Watanabe, Y.; Nakamura, Y. *J. Mater. Sci.* **2002**, *37*, 3585−3587.
(27) Edri, E.; Kirmayer, S.; Cahen, D.; Hodes, G. *J. Phys. Chem. Lett.* **2013**, 897−902.
(28) Edri, E.; Kirmayer, S.; Kulbak, M.; Hodes, G.; Cahen, D. *J. Phys. Chem. Lett.* **2014**, 429−433.
(29) Stoumpos, C. C.; Malliakas, C. D.; Kanatzidis, M. G. *Inorg. Chem.* **2013**, *52*, 9019−9038.
(30) Huheey, J. *Inorganic Chemistry Principles of Structure and Reactivity*; 4th ed.; Prentice Hall: Upper Saddle River, NJ, 1997.

(31) Cui, H.; Hodgdon, T. K.; Kaler, E. W.; Abezgauz, L.; Danino, D.; Lubovsky, M.; Talmon, Y.; Pochan, D. J. *Soft Matter* **2007**, *3*, 945.
(32) Friedrich, H.; Frederik, P. M.; de With, G.; Sommerdijk, N. A. J. M. *Angew. Chem., Int. Ed.* **2010**, *49*, 7850−7858.
(33) Ball, J. M.; Lee, M. M.; Hey, A.; Snaith, H. J. *Energy Environ. Sci.* **2013**, *6*, 1739−1743.
(34) Tan, K. W.; Moore, D. T.; Saliba, M.; Sai, H.; Estroff, L. A.; Hanrath, T.; Snaith, H. J.; Wiesner, U. *ACS Nano* **2014**, *8*, 4730−4739.
(35) Baikie, T.; Fang, Y.; Kadro, J. M.; Schreyer, M. K.; Wei, F.; Mhaisalkar, S. G.; Gratzel, M.; White, T. *J. Mater. Chem. A* **2013**, *1*, 5628−5641.
(36) Ryu, S.; Noh, J. H.; Jeon, N. J.; Kim, Y. C.; Yang, W. S.; Seo, J. W.; Seok, S. I. *Energy Environ. Sci.* **2014**, *7*, 2614−2618.